Model establishment and microarray analysis of mice with oxaliplatin-induced hepatic sinusoidal obstruction syndrome

CHEN ZHU[1*], XINWEI CHENG[1*], PING GAO[2], QIANYAN GAO[1], XIMIN WANG[1],
DONG LIU[1], XIUHUA REN[1] and CHENGLIANG ZHANG[1]

[1]Department of Pharmacy, Tongji Hospital; [2]Department of Pharmacy, Wuhan Children's Hospital, Tongji Medical College,
Huazhong University of Science and Technology, Wuhan, Hubei 430030, P.R. China

Abstract. Hepatic sinusoidal obstruction syndrome (HSOS) is a serious side effect of oxaliplatin (OXA) treatment. The present study aimed to establish a reproducible mouse model of OXA-induced HSOS and to preliminarily explore the underlying molecular mechanisms using mRNA microarray analysis. A total of 45 C57BL/6 male mice were randomly divided into five groups: Control, 5 mg/kg OXA, 10 mg/kg OXA, 15 mg/kg OXA and 20 mg/kg OXA. The mice were respectively injected intraperitoneally with 5% glucose solution, or 5, 10, 15 or 20 mg/kg OXA solution once a week for 6 consecutive weeks. The body weight of the mice was recorded every day. The serum levels of alanine aminotransferase (ALT) and aspartate aminotransferase (AST) were determined. Hematoxylin and eosin staining, Sirius red staining and scanning electron microscopy were used to identify pathological changes. mRNA microarray was used to analyze changes in the gene expression profiles mainly from the functional aspects of Gene Ontology and the Kyoto Encyclopedia of Genes and Genomes. The oxidation mechanism was verified by measuring oxidative stress-related markers and reactive oxygen species with dihydroethidium probe technology, according to the microarray results. Among all of the OXA groups, 10 mg/kg OXA resulted in an acceptable survival rate of 78%. The mice showed obvious splenomegaly, increases in serum levels of ALT and AST, aggravation of liver pathological injuries and hepatic sinusoidal injuries. The microarray results suggested that mRNA expression changes after OXA treatment were associated with 'oxidative stress', 'coagulation function', 'steroid anabolism' and 'pro-inflammatory responses'. The results confirmed that OXA aggravated oxidative damage in the livers of the mice. The present study successfully established a mouse model of OXA-induced HSOS and preliminarily analyzed the underlying molecular mechanisms involved, thus laying a foundation for a subsequent in-depth study.

Introduction

Colorectal cancer (CRC) is currently one of the most common types of gastrointestinal cancer. Its incidence rate ranks third among all types of gastrointestinal cancer (1), seriously affecting human life and health. Oxaliplatin (OXA) was initially marketed in France in 1996 and can inhibit the DNA synthesis of tumor cells to prevent their division and proliferation, thereby causing toxic effects (2). Currently, a combined chemotherapy regimen of OXA, 5-fluorouracil and leucovorin is the main treatment for stage III and metastatic CRC (2-6). However, the wide use of OXA in cancer treatment has resulted in adverse effects involving neurotoxicity, bone marrow suppression and liver toxicity, seriously affecting chemotherapy and the quality of life of the patients (7-9).

In 2004, it was reported that 79% of the patients with metastatic colorectal cancer undergoing OXA-containing chemotherapy had hepatic sinusoidal injuries (10). OXA-induced hepatic sinusoidal obstruction syndrome (HSOS) has become a major concern for patients with CRC receiving chemotherapy with OXA. OXA can cause edema and continuous disintegration of liver sinusoidal endothelial cells (LSECs). The damaged LSECs can secrete cytokines that induce weakness of the mucosal barrier between the LSECs, thus resulting in the escape of red blood cells, white

Correspondence to: Dr Xiuhua Ren or Dr Chengliang Zhang, Department of Pharmacy, Tongji Hospital, Tongji Medical College, Huazhong University of Science and Technology, 1095 Jiefang Avenue, Wuhan, Hubei 430030, P.R. China
E-mail: 271052026@qq.com
E-mail: clzhang@tjh.tjmu.edu.cn

*Contributed equally

Abbreviations: ALT, alanine aminotransferase; AST, aspartate aminotransferase; CAT, catalase; CRC, colorectal cancer; DEG, differentially expressed genes; DHE, dihydroethidium; GO, Gene Ontology; GSH, reduced glutathione; H&E, hematoxylin and eosin; HSOS, hepatic sinusoidal obstruction syndrome; KEGG, Kyoto Encyclopedia of Genes and Genomes; LSEC, liver sinusoidal endothelial cell; MDA, malondialdehyde; OXA, oxaliplatin; ROS, reactive oxygen species; SEM, scanning electron microscopy; SOD, superoxide dismutase

Key words: HSOS, model, mRNA microarray, OXA, oxidative stress

blood cells and platelets into the space of Disse between the hepatocytes and sinusoidal ECs and leading to dissection of Disse. The cascade of actions, and the activation of the healing mechanism resulting in fibrosis, lead to normal blood flow obstruction and increased venous resistance, thus resulting in the development of high portal blood pressure, further liver dysfunction and ascites (11). Notably, the pathological characteristics of OXA-induced HSOS mainly include sinusoidal dilatation, sinusoidal obstruction and peripheral lobular vein fibrosis (12,13). Patients with CRC undergoing OXA-based chemotherapy who develop sinusoidal injury and do not receive timely intervention may further develop liver fibrosis and cirrhosis (14). Previous studies have demonstrated that in patients with CRC that experience OXA-induced HSOS following partial hepatectomy, their liver function reserve is significantly reduced and some patients may even develop liver failure, which greatly aggravates the course of the disease after hepatectomy (9,15,16). In addition to liver damage, OXA-induced HSOS is associated with higher rates of overall morbidity, bleeding risk, decreased tumor response and longer hospital stays (15-17).

Although a number of clinical reports have proven the universality of OXA-induced HSOS (10,13,18,19), little is known about its pathogenesis and therapeutic drugs to treat the disease are scarce. An important reason for this is the lack of recognized animal models, which limits the development of studies to investigate the mechanisms involved. Therefore, in the present study, a mouse model of OXA-induced HSOS was established and the possible pathological mechanisms were preliminarily analyzed using mRNA microarray analysis to provide a basis for future research on the intervention of OXA-induced HSOS.

Materials and methods

Animals and treatments. A total of 45 male C57BL/6 mice (weight, 20±2 g; age, 8-10 weeks) were obtained from Sipeifu (Beijing) Biotechnology Co., Ltd. All animals were maintained at 23±2˚C and 65±5% humidity, under a 12-h light/dark cycle, and were provided with free access to standard laboratory food and water. The present study was approved by the Animal Experiment Ethics Committee of Tongji Medical College, Huazhong University of Science and Technology (Wuhan, China; approval no. 2646). The experimental animals were provided with humane care in accordance with the institutional animal care guidelines (20). Humane endpoints were in place where animals would be sacrificed if they had lost 20% weight or exhibited 10% weight loss alongside hypotrichosis, anorexia or decreased vitality decreases.

The 45 C57BL/6 male mice were randomly divided into the following five groups: i) Control, ii) 5 mg/kg OXA, iii) 10 mg/kg OXA, iv) 15 mg/kg OXA and v) 20 mg/kg OXA (n=9/group). Mice in the different OXA groups were injected intraperitoneally with 5, 10, 15 or 20 mg/kg OXA solution once a week for 6 consecutive weeks. Mice in the control group were given a corresponding volume of 5% glucose solution (0.02 ml/g) each time. Each day, the behaviors and health of mice were monitored and the body weight was recorded. After the last administration, the mice were fasted but had access to water overnight before sacrifice. All of the mice were sacrificed via cervical dislocation under anesthesia with an initial intraperitoneal injection of sodium pentobarbital (30 mg/kg body weight) to minimize animal suffering. Mice whose breathing and heartbeat had stopped were considered to have succumbed. Blood samples was collected from orbital venous plexus before anesthesia. Liver tissues and spleen tissues were collected and weighed for subsequent analyses.

Serum biochemistry analysis. The blood samples was placed in EP tubes at room temperature for 1 h and then centrifuged at 855 x g for 10 min, and the supernatant was taken to obtain the serum. Commercial kits (Nanjing Jiancheng Institute of Biological Engineering) were used to determine the serum levels of aspartate aminotransferase (AST, cat. no. C009-3-1) and alanine aminotransferase (ALT, cat. no. C010-3-1) in the mice from each experimental group in strict accordance with the manufacturer's instructions.

Liver histological analyses. The mice livers were removed, washed with sterile saline and fixed in 10% neutral formaldehyde at room temperature for 48 h. The tissue samples were then dehydrated and embedded in paraffin. The paraffin blocks were sectioned at a thickness of 4 μm and each section was stained with hematoxylin and eosin (H&E) at room temperature for 5 mins. Pathological changes in the livers were observed under an optical microscope (Thermo Fisher Scientific, Inc.).

For Sirius red staining, at room temperature, sections were first stained with celestine blue solution for 5-10 min, then with Sirius red-saturated picric acid for 15-30 min. After sealing with neutral glue, the sections were observed under an optical microscope (Thermo Fisher Scientific, Inc.).

For scanning electron microscopy (SEM), liver tissue was harvested within 1-3 min after the mice were sacrificed. Liver tissue was fixed in 2.5% glutaraldehyde (Structure Probe, Inc.) at room temperature for 2 h and then transferred to 4˚C for storage. After repeated washing with 0.1 M phosphate buffer, fixed samples were prepared with 1% osmic acid at room temperature and protected from light for 1-2 h. Subsequently, the samples were sequentially dehydrated in alcohol and isoamyl acetate of different concentrations. After drying, each sample was coated by ion sputtering and observed by SEM (Hitachi, Ltd.).

mRNA microarray sample processing. A total of four liver tissue samples/group was randomly selected from mice in the control group and the 10 mg/kg OXA group. Total RNA was extracted from the tissues using Takara RNAiso Plus (cat. no. 9109; Takara Bio, Inc.). After passing an electrophoretic quality inspection (Agilent Technologies, Inc.), the extracted total RNA was purified using RNeasy Mini kit and an RNase-free DNase kit (Qiagen GmbH). The total RNA of the samples was amplified and labeled using the Agilent Expression Profile Chip kit (Agilent Technologies, Inc.) and then the labeled cRNA was purified by RNeasy Mini kit (Qiagen GmbH). Each slide was hybridized with 1.65 μg Cy3-labeled cRNA using Gene Expression Hybridization Kit (Agilent Technologies, Inc.) in Hybridization Oven (Agilent Technologies, Inc.), according to the manufacturer's instructions After 17 h hybridization, slides were washed in staining dishes (Thermo Shandon, Waltham)

with Gene Expression Wash Buffer Kit (Agilent technologies, Inc.), followed the manufacturer's instructions. The slides that completed hybridization were scanned by an Agilent micro-array scanner (Agilent Technologies, Inc.). The data were extracted using Feature Extraction software 10.7 (Agilent Technologies, Inc.). The 'limma' package in R (https://www.rdocumentation.org/packages/limma/versions/3.28.14) was used to normalize the raw data by the quantile algorithm. Normalized data were screened by a fold-change statistical method using the following selection conditions: Fold-change (linear) ≤0.5 or fold-change (linear) ≥2. In addition, the normalized data were processed by a boxplot, sample cluster map, sample correlation analysis, principal component analysis (PCA), scatter plot, volcano plot and cluster heatmap using 'ggplot2' package in R (https://www.rdocumentation.org/packages/ggplot2/versions/3.3.6). Technical support was provided by Shanghai Bohao Biotechnology Co., Ltd.

Functional enrichment analysis of differentially expressed mRNA. Through Gene Ontology (GO; geneontology.org) and Kyoto Encyclopedia of Genes and Genomes (KEGG; genome.jp/kegg) enrichment analyses, differentially expressed genes (DEGs) were classified based on different functions. The adopted method is fisher exact test, and the data packet is cluster Profiler from R/bioconductor (https://bioconductor.org/packages/release/bioc/html/clusterProfiler.html); The selection criterion is that the number of DEGs on a certain GO term or KEGG pathway is ≥2 and the P-value is <0.05. The GO terms and KEGG pathways were obtained, presented in descending order according to the enrichment factor values, and the top 30 results were assessed in the present study. Enrichment factor was calculated as follows: Enrichment factor=(the number of DEGs in a term/the total number of DEGs)/(the total number of genes in the database term/the total number of genes in the database).

Reverse transcription quantitative polymerase chain reaction (RT-qPCR). Total RNA was isolated from liver samples obtained from the mice in 10 mg/kg OXA group and control group using TRIzol® reagent (Invitrogen; Thermo Fisher Scientific, Inc.). RNA samples were quantified and the purity was assessed using a NanoDrop BioChrom apparatus (Harvard Bioscience). A total of 1 µg RNA was isolated and reverse transcribed to cDNA using PrimeScript™ RT Master Mix (Takara Biotechnology Co., Ltd.) at 37˚C for 15 mins and 95˚C for 5 sec. qPCR was performed using SYBR Green (Takara, Dalian, China) on an Applied Biosystems StepOnePlus Real-time PCR system (Applied Biosystems). qPCR cycle parameters were as follows: 95˚C for 5 min, followed by 40 cycles at 95˚C for 10 sec and 60˚C for 30 sec, and extension at 72˚C for 20 sec. A final extension step at 72˚C for 10 min was conducted. Results were obtained with Bio-Rad CFX Manager (Bio-Rad Laboratories, Inc.) and were analyzed using the $2^{-\Delta\Delta Cq}$ method (21) with the β-actin gene used as the endogenous control. The PCR primers are listed in Table I.

Analysis of oxidative stress indexes. At 4˚C, mouse liver tissue homogenates (10%) were prepared by adding nine volumes (ml) of normal saline to the liver mass (g)=1/9 and centrifuging for 10 min at 627-1,164 x g; the supernatant

Table I. Sequence of primers used for quantitative polymerase chain reaction.

Gene name	Sequence (5'-3')
Fmo3	F: GGCCTGTGGAAATTCTCAGAC
	R: AAGTCATCGGGATAGGGGAAG
Sult1e1	F: ATGGAGACTTCTATGCCTGAGT
	R: ACACAACTTCACTAATCCAGGTG
9530077C05Rik	F: TCTATTCGCGTAACGGAAAAGC
	R: TGAGAATCCCAGAGGACAAACTC
Cyp2b9	F: GCTCATTCTCTGGTCAGATGTTT
	R: CGCTTGTGGTCTCAGTTCCA
Sult3a2	F: GACCCACGAGCAAACAATGAA
	R: TCCAGTCTCCAACGATACCTT
Hsd3b5	F: GCTCTTGGAAACAAAAGGAAC ACT
	R: TTCGACCGAAGGTCCTGAAC
Hsd3b4	F: GAGGTTTCTCATAAGCACAGG AGT
	R: TCCTCCTGCACCAACATTCG
Elovl3	F: TTCTCACGCGGGTTAAAAATGG
	R: GAGCAACAGATAGACGACCAC
Slco1a1	F: GTGCATACCTAGCCAAATCACT
	R: CCAGGCCCATAACCACACA
Ugt2b38	F: TGCGCCACAAAAGGGCTAA
	R: ACACAAGAGAGTAGGAAGCCG
β-actin	F: GGCTGTATTCCCCTCCATCG
	R: CCAGTTGGTAACAATGCCATGT

F, forward; R, reverse.

was used for subsequent analyses. The malondialdehyde (MDA, cat. no. A003-1-2), superoxide dismutase (SOD, cat. no. A001-3-2), reduced glutathione (GSH, cat. no. A006-2-1) and catalase (CAT, cat. no. A007-1-1) levels in the mice livers of each experimental group were measured according to the kit instructions (Nanjing Jiancheng Bioengineering Institute), in order to evaluate the oxidative stress-related damage in the mice livers.

Staining of dihydroethidium (DHE)-reactive oxygen species (ROS). Frozen liver sections (-26˚C; 6 µm thickness) were warmed at room temperature and mounted with an anti-fluorescence quenching solution for 5 min. ROS dye solution (cat. no. D7008; MilliporeSigma) was added dropwise and sections were incubated for 30 min at 37˚C in the dark. Subsequently, the sections were washed three times with phosphate-buffered saline (PBS, pH 7.4) and DAPI staining solution (Beijing Solarbio Science & Technology Co., Ltd.) was added dropwise and incubated for 10 min at room temperature in the dark. After washing three times with PBS and drying, the sections were mounted with an anti-fluorescence quenching solution. The sections were observed under a fluorescence microscope (Nikon Corporation) and images were captured.

Statistical analysis. GraphPad Prism 8.0 software (GraphPad Software, Inc.) was used for the statistical analyses. The data are presented as the mean ± standard deviation. Data between groups were analyzed by one-way ANOVA followed by Dunnett's post hoc test. $P<0.05$ was considered to indicate a statistically significant difference.

Results

OXA-induces HSOS in mice. To explore the optimal dose of OXA in the mouse model, the present study selected 5, 10, 15 and 20 mg/kg OXA based on previous reports and the clinical dose (22-26). It was found that 3 weeks after the start of the experiment, all mice in the 20 mg/kg OXA group and seven mice in the 15 mg/kg OXA group met the humane endpoints before the end of the experiment. No mice succumbed in the control group or the 5 mg/kg OXA group and only two mice met the humane endpoints and were sacrificed in the 10 mg/kg OXA group at the fifth week (Fig. 1A). Therefore, subsequent experiments were mainly performed in these three groups. Compared with in the control group, the body weight of the mice in the 5 and 10 mg/kg OXA groups were decreased following the administration of OXA (Fig. 1B) $(P<0.01)$ and body weight in the 10 mg/kg OXA group decreased more than that in 5 mg/kg OXA group, but the difference was not statistically significant.

Liver changes and basic biochemical indexes showed that the liver weight ratio, and serum levels of ALT and AST, which are common indicators of liver injury (Fig. 1C, E, G and H), were increased after OXA treatment and the changes were more significant in the 10 mg/kg OXA group $(P<0.01)$. Splenomegaly is closely related to OXA-induced HSOS (17,27) and can be used as a reliable predictor of the occurrence and severity of OXA-induced HSOS (28). In the present study, the ratio of spleen weight to body weight in the different OXA groups showed a dose-dependent increase compared with that in the control group (Fig. 1D and F).

Next, the pathological changes in the livers were analyzed. H&E staining of the liver tissue of mice in the control group did not show evident abnormalities. The livers of the mice in the 5 mg/kg OXA group showed mild dilatation of hepatic sinusoids. Furthermore, the mice livers in the 10 mg/kg OXA group showed more serious injuries and there was marked dilatation of hepatic sinusoids around the central vein and increased hepatocyte spaces (Fig. 2). Next, liver fibrosis was determined using Sirius red staining, which showed that liver fibrosis was very mild in mice administered 5 mg/kg OXA. In addition, the staining of the mice livers was more intense and the collagen deposition increased after the administration of 10 mg/kg OXA, thereby indicating that 10 mg/kg OXA exacerbated fibrotic changes in the mice livers (Fig. 2). Moreover, SEM showed that OXA resulted in obvious damage to the mice liver sinusoids in a dose-dependent manner, resulting in the enlargement of hepatic sinusoidal endothelial spaces and expansion of the fenestra (Fig. 2).

Taken together, these results indicated that 10 mg/kg OXA could cause obvious liver damage, fibrosis and hepatic sinusoidal dilation without excessive death. Therefore, it was decided that 10 mg/kg OXA could be used for the modeling of OXA-induced HSOS.

Changes in the mRNA expression profile in the livers of a mouse model of OXA-induced HSOS. To observe genetic changes in the pathological process of OXA-induced HSOS, microarray technology was used to determine the mRNA expression profiles in the mice livers in the OXA (10 mg/kg) group and the control group. First, the differences in the characteristics of the two groups were analyzed and presented in a PCA diagram (Fig. 3A), cluster diagram (Fig. 3B) and pearson correlation analysis diagram (Fig. 3C). In the comparison of data between the control group and the 10 mg/kg OXA group, the genes in the livers of the mice in the two groups were not well correlated, whereas those within the same group were correlated. Thus, the mRNA expression in the liver samples from OXA-induced HSOS mice was significantly different from that in the livers of mice in the control group.

Next, the distribution of DEGs between the samples of the two groups was analyzed and presented in a scatter plot, volcano plot and heat map. As shown in Fig. 4, the distribution concentration trend of data in the two groups was significantly different. Genes with a similar expression clustered together with the samples and DEGs between the two groups showed different expression levels, thereby further indicating that the changes in gene expression in the mice liver samples after OXA administration were significantly different from those in the livers of mice in the control group (Fig. 4A-C). A total of 1,109 DEGs were identified, including 512 downregulated genes and 597 upregulated genes. The top five downregulated and top five upregulated DEGs are listed in Table II. To confirm the reliability of the microarray data, the mRNA expression levels of these candidate genes were investigated by RT-qPCR. The $2^{-\Delta\Delta Cq}$ levels and $\log_{10}$ fold change of each of the 10 genes were listed in Table III. The results were consistent with those from the microarray data (Fig. 4D and E).

GO and KEGG pathway analysis. By performing GO enrichment analysis of DEGs, genes can be classified based on different functions to achieve the purpose of annotation and classification of the genes (29). As shown in Fig. 5, DEGs between the control group and 10 mg/kg OXA group were mostly enriched in biological processes (Fig. 5A). In addition, the GO analysis of the top 30 enrichment factors showed that DEGs were mainly enriched in 'steroid hydroxylase activity', 'oxidoreductase activity, acting on paired donors', 'integrin complex', 'arachidonic acid monooxygenase activity' and 'arachidonic acid epoxygenase activity' (Fig. 5B).

KEGG enrichment analysis of the DEGs showed the enrichment levels of the these genes in different pathways (29), which may identify the biological regulatory pathways that were significantly different under the experimental conditions. The results provided directions for subsequent research on identifying the underlying mechanisms involved. According to the KEGG enrichment results, most of the enriched pathways were related to human diseases (Fig. 6A). Compared with the control group, the enriched pathways of DEGs in the 10 mg/kg OXA group were mainly involved in 'steroid hormone biosynthesis', 'retinol metabolism', 'PPAR signaling pathway', 'inflammatory mediator regulation of TRP channels', 'glutathione metabolism', 'drug metabolism-other enzymes', 'drug metabolism-cytochrome P450' and 'arachidonic acid metabolism' (Fig. 6B).
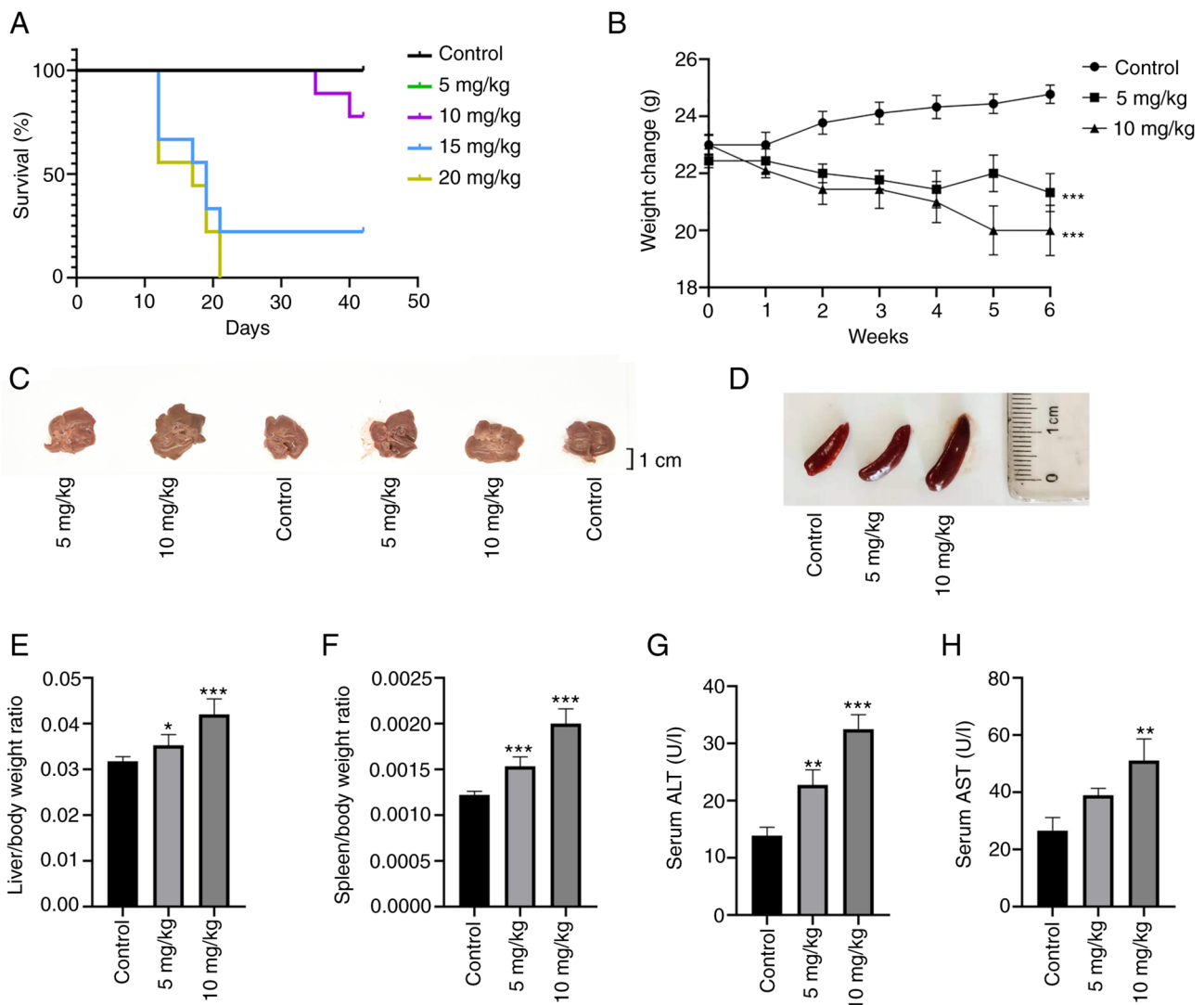
Figure 1. OXA-induced HSOS in mice. (A) Survival rate of mice after i.p. treatment with OXA. (B) Body weight after i.p. treatment with OXA. (C) Changes in the liver. (D) Changes in the spleen. (E) Liver weight-to-body weight ratio. (F) Spleen weight-to-body weight ratio. Serum levels of (G) ALT and (H) AST. The results are shown as the mean ± standard deviation for each group and were analyzed with a one-way ANOVA followed by Dunnett's post hoc test. [*]P<0.05, [**]P<0.01 and [***]P<0.001 vs. control group. OXA, oxaliplatin; HSOS, hepatic sinusoidal obstruction syndrome; i.p., intraperitoneal; ALT, alanine aminotransferase; AST, aspartate aminotransferase.

Oxidative stress-related indicators in OXA-induced HSOS in mice. The microarray results suggested that oxidative stress may serve an important role in OXA-induced HSOS. Therefore, the levels of common oxidative stress markers were determined and changes in ROS were observed by DHE staining. MDA is a lipid peroxidation product *in vivo*, which can cause cytotoxicity (30). The MDA levels in the mice livers were significantly increased following the administration of 10 mg/kg OXA (P<0.05; Fig. 7A). SOD is an antioxidant metal enzyme that can catalyze the superoxide anion radical and provide cellular defenses against ROS (22). CAT is also an antioxidant enzyme that protects cells from the toxicity of H_2O_2 (22). GSH has antioxidant and integrative detoxification effects (22). OXA markedly reduced the levels of SOD, CAT and GSH in the mice livers (P<0.05; Fig. 7B-D). Furthermore, DHE probe technology was used to analyze changes in ROS levels. The results showed that the ROS levels in the livers of the mice in the OXA group were increased in a dose-dependent manner (Fig. 7E). Taken together, these data confirmed that

oxidative stress may have an important role in the liver damage of mice with OXA-induced HSOS.

Discussion

The main side effects of OXA are neurotoxicity, bone marrow suppression and gastrointestinal reaction. Recently, hepatic sinusoidal injury has garnered attention as a hepatotoxic reaction that occurs in patients with CRC liver metastases after receiving OXA-based neoadjuvant chemotherapy, with a worldwide incidence rate of 48-79% (10,31,32). The typical pathological features of OXA-induced HSOS include hepatic sinusoidal dilatation, platelet aggregation in the hepatic sinusoids and some typical clinical features, such as blue liver, splenomegaly and thrombocytopenia (33). A number of clinical reports have proven the universality of OXA-induced HSOS, which usually only focused on clinical features and diagnosis (10,13,18,19). Reports on the mechanism of its pathogenesis are limited. There is currently no recognized OXA-induced hepatotoxicity model.
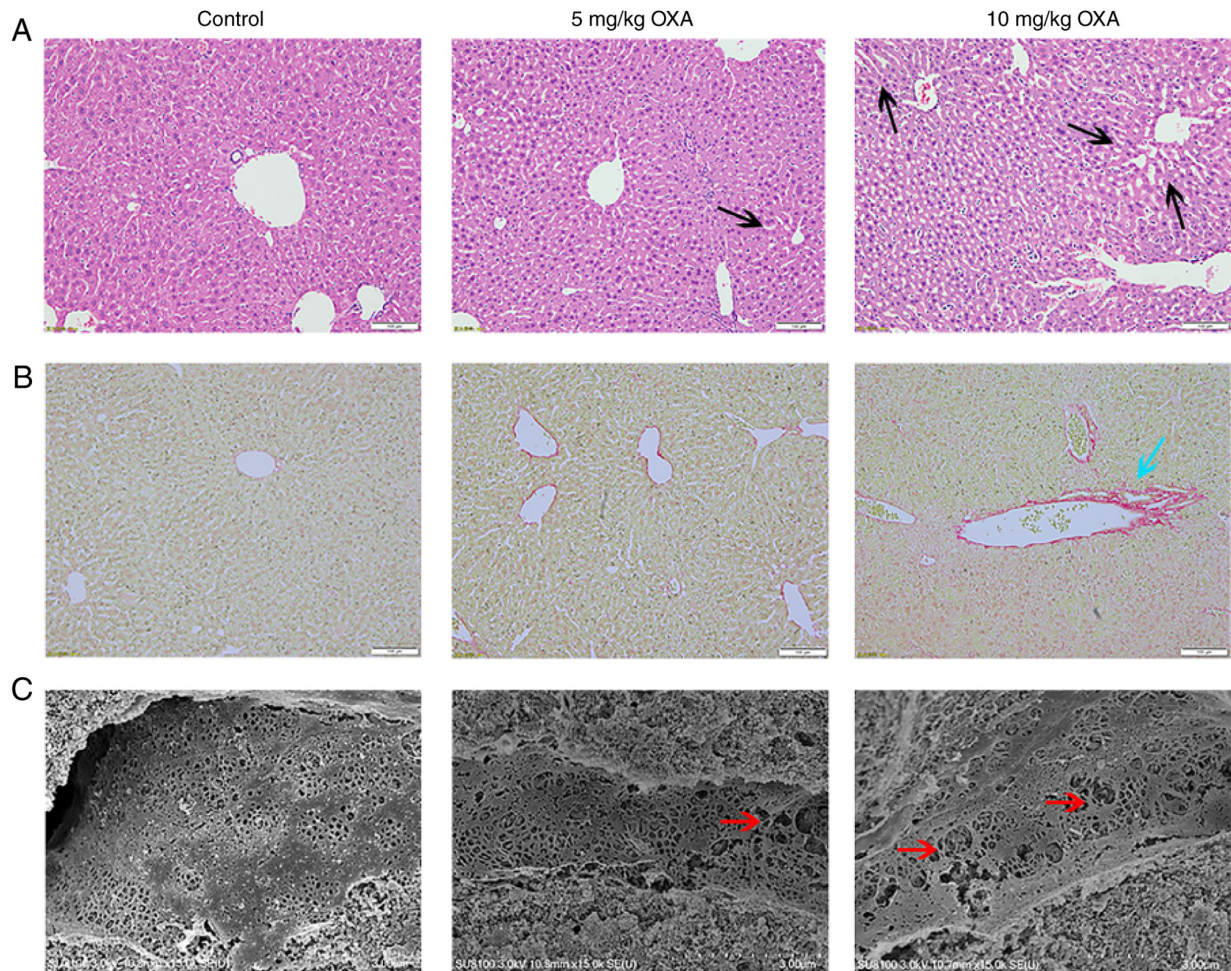
Figure 2. Pathological changes in the liver of mice with OXA-induced hepatic sinusoidal obstruction syndrome. (A) Hematoxylin and eosin staining (magnification, x100; scale bar=100 µm). (B) Sirius red staining (magnification, x100; scale bar=100 µm). (C) Scanning electron microscopy (magnification, x15,000; scale bar=3 µm). Black arrow, hepatic sinusoidal dilatation; blue arrow, collagen deposition; red arrow, enlargement of hepatic sinusoidal endothelial fenestra. OXA, oxaliplatin.

In previous studies on OXA-induced hepatotoxicity, the doses of OXA ranged between 5 and 30 mg/kg (26,34-36). In the present study, a gradient of OXA doses for modeling was screened and it was revealed that the mortality rate of mice in the 15 and 20 mg/kg OXA groups reached 78-100%, which indicated a strong toxic reaction from high-dose OXA. Furthermore, the present study showed that a suitable HSOS model with an acceptable survival rate could be established after 6 weeks of 10 mg/kg OXA administration. The OXA dose the present study recommended for HSOS modeling was much lower than the dose presented in other studies (34,35). It was hypothesized that this difference may be due to the dosing frequency and modeling time. According to the National Comprehensive Cancer Network guidelines, the optimal duration of OXA plus 5-fluorouracil and leucovorin or oral fluoropyrimidine (capecitabine) in patients with CRC is 3 or 6 months, with a cycle of 2 weeks (37). Instead of the continuous daily administration used in other studies (23,38), the present study decided to administer OXA by intraperitoneal injection once a week for 6 consecutive weeks to simulate the clinical protocol (22). Which also took into consideration the growth cycle of the mice.

Nam *et al* (12) demonstrated that patients with CRC who received OXA chemotherapy were more likely to have abnormal liver functions, and increased serum levels of AST, ALT and total bilirubin. The results of the present study showed that after the long-term administration of 10 mg/kg OXA, the body weight of the mice decreased significantly, whereas the liver weight-to-body weight ratio, and the serum levels of ALT and AST were increased. Overman *et al* (17) revealed that liver sinusoidal injury caused by OXA-based chemotherapy may cause a dose-dependent increase in spleen volume. El Chediak *et al* (28) reported that an increase in spleen volume was an independent predictor of HSOS in 79 patients treated with OXA. The current study revealed that the spleens were enlarged in mice in the 10 mg/kg OXA group compared with in the control group, which was consistent with the clinical characteristics of patients with cancer and OXA-induced HSOS.

HSOS is a clinical syndrome in which hepatic sinusoidal endothelial cells are shed by drugs or toxins, resulting in the obstruction of the hepatic outflow tract and downstream hepatic small veins, thus leading to intrahepatic pre-sinusoidal or post-sinusoidal portal hypertension in patients who undergo chemotherapy (39). Rubbia-Brandt *et al* (13) showed that
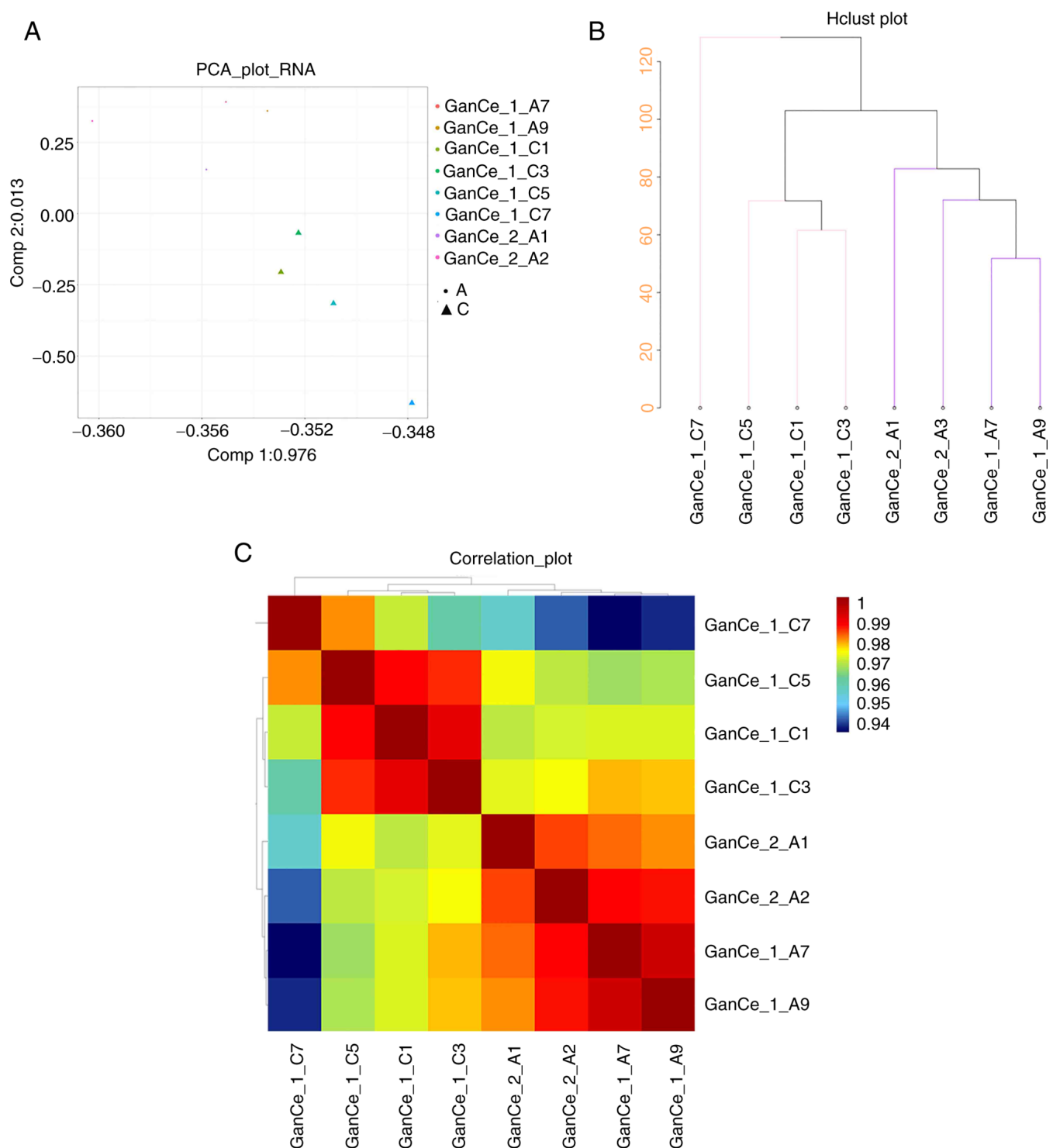
Figure 3. Differences in characteristics of the mRNA expression profiles in the livers of mice with OXA-induced hepatic sinusoidal obstruction syndrome. (A) PCA diagram. (B) Cluster diagram. (C) Correlation analysis diagram. Data are shown for mice in the control and 10 mg/kg OXA groups. OXA, oxaliplatin; PCA, principal component analysis.

the pathology of liver tissue resected from 274 patients with CRC liver metastases treated with OXA-based chemotherapy exhibited hepatic sinusoidal dilation and obstruction, nodular changes in the liver, hepatic lobular central fibrosis, hepatocyte steatosis and hemorrhage. To further confirm liver changes in mice with OXA-induced HSOS, in addition to basic histological staining analysis, the present study performed SEM to observe the changes in hepatic sinusoids in mice, which is an important

indicator of whether OXA-induced HSOS has been produced. The results showed hepatic sinusoidal dilatation and increased hepatocyte space following treatment with OXA and the severity of the liver injury was proportional to the dose of OXA received. SEM analysis showed that OXA treatment resulted in the enlargement of hepatic sinusoidal endothelial spaces and expansion of the fenestra. The results confirmed that an OXA-induced HSOS model was successfully established with typical pathological
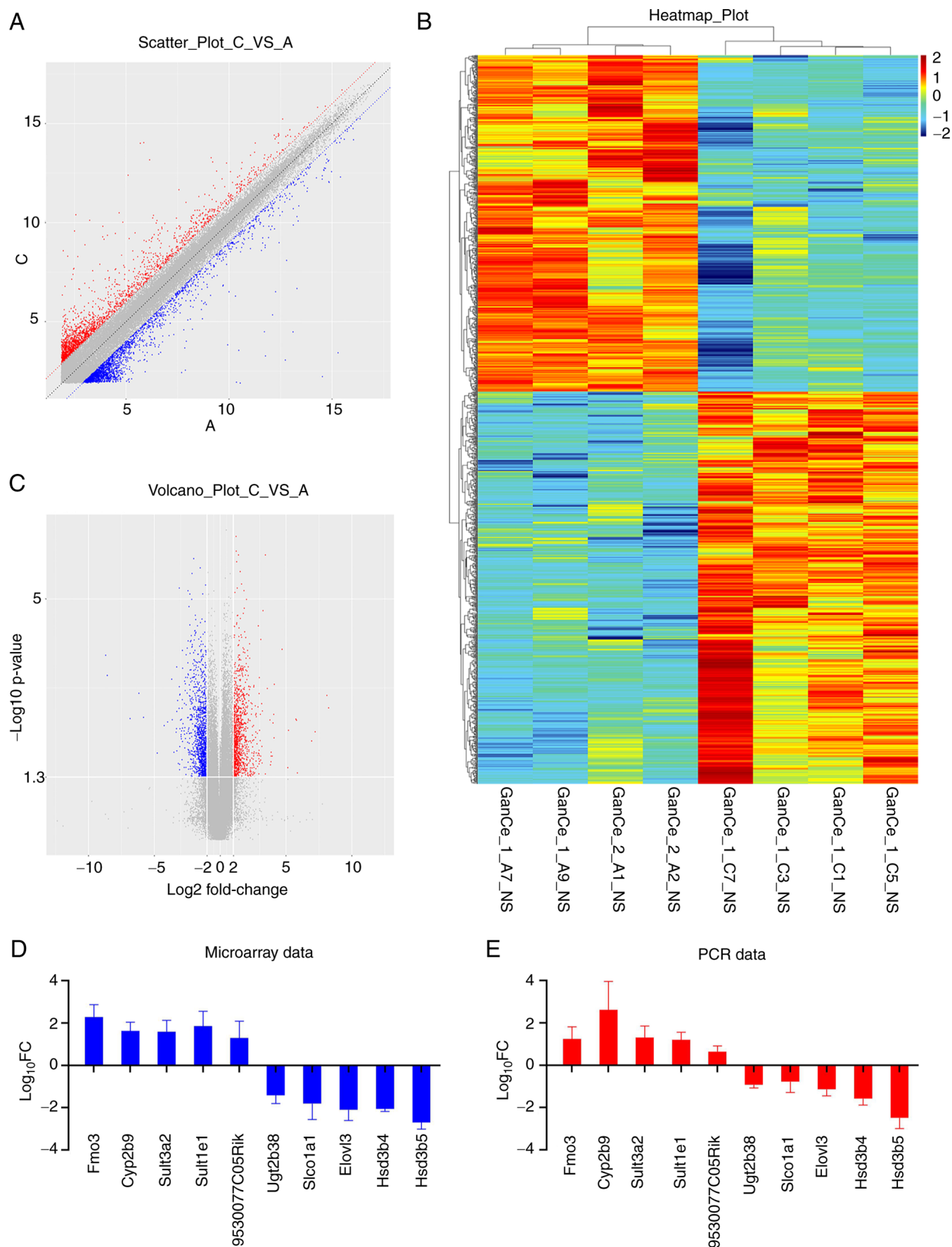
Figure 4. mRNA expression profiles in the livers of mice with OXA-induced hepatic sinusoidal obstruction syndrome. (A) Scatter plot. Red dots, 2-fold upregulated genes; blue dots, 2-fold downregulated genes. (B) Heat map. (C) Volcano plot. Red dots, genes with P-value <0.05 and FC ≥2; blue dots, genes with P-value <0.05 and FC ≤0.5. Data are shown for mice in the control and 10 mg/kg OXA groups. (D) Microarray data of the top five downregulated and top five upregulated differentially expressed genes. (E) Reverse transcription-quantitative PCR confirmation for the top five downregulated and top five upregulated differentially expressed genes. OXA, oxaliplatin; FC, fold change; PCR, polymerase chain reaction.

Table II. Microarray analysis of top five downregulated and upregulated DEGs.

A, Upregulated genes

Gene symbol	Log$_{10}$ FC	P-value
Fmo3	2.4939	0.0018
Sult1e1	2.1863	0.0057
9530077C05Rik	1.7790	0.0411
Cyp2b9	1.7591	0.0033
Sult3a2	1.7457	0.0031

B, Downregulated genes

Gene symbol	Log$_{10}$ FC	P-value
Hsd3b5	-2.6038	0.0001
Hsd3b4	-2.0468	0.0031
Elovl3	-1.8459	0.0009
Slco1a1	-1.4250	0.0159
Ugt2b38	-1.2663	0.0043

DEGs, differentially expressed genes; FC, fold change.

Table III. Polymerase chain reaction variation of top five downregulated and upregulated DEGs.

A, Upregulated DEGs

Gene symbol	$2^{-\Delta\Delta Cq}$	Log$_{10}$ FC	P-value
Fmo3	17.354	1.239	0.0026
Cyp2b9	410.518	2.613	0.0003
Sult3a2	19.962	1.300	0.0014
Sult1e1	15.666	1.195	0.0088
9530077C05Rik	4.396	0.643	0.0192

B, Downregulated DEGs

Gene symbol	$2^{-\Delta\Delta Cq}$	Log$_{10}$ FC	P-value
Hsd3b5	0.003	-2.492	0.0001
Hsd3b4	0.026	-1.585	0.0015
Elovl3	0.072	-1.145	0.0079
Slco1a1	0.166	-0.780	0.0312
Ugt2b38	0.117	-0.931	0.0217

DEGs, differentially expressed genes; FC, fold change.

characteristics. In addition, liver fibrosis was also found in mice in the 10 mg/kg group, which may aggravate the course of liver injury and prolong its recovery time (16). Based on these results, a typical HSOS model could be established after 6 weeks of OXA administration at a dose of 10 mg/kg.

In a previous study, a preliminary analysis was performed based on the comparison of gene expression profiles of 11 human livers with OXA-induced HSOS and 12 histologically normal livers (25). The main genes in the following pathways were upregulated in patients with HSOS: Acute-phase reaction, coagulation system disorder, liver fibrosis and oxidative stress (25). However, in this previous study, only a simple microarray analysis of a few genes was made and the study lacked an analysis of the mechanism of the pathways involved. In addition, to the best of our knowledge, no mRNA microarray study on an animal model of OXA-induced HSOS has been performed. Therefore, the present study used mRNA microarray technology to explore changes in the gene expression profiles of livers with OXA-induced HSOS, hoping to provide possible directions for subsequent studies of the disease mechanism. The GO database classifies gene function into three broad categories: Cellular components, molecular functions and biological processes. The present study proved that DEGs between the control group and the 10 mg/kg OXA group were expressed in all three categories but were mainly concentrated in the biological processes category. Among the top 30 enriched GO terms, the DEGs were mainly enriched in 'steroid hydroxylase activity', 'oxidoreductase activity, acting on paired donors', 'integrin complex', 'arachidonic acid mono-oxygenase activity' and 'arachidonic acid epoxygenase activity'. The integrin complex connects the extracellular matrix and the cytoskeleton, controls intracellular signal events related to proliferation, differentiation, migration and other cellular processes (40), and may be involved in the regulation of fibrosis (41). OXA has been reported to accelerate the activation of hepatic stellate cells and collagen synthesis by upregulating the expression of type I collagen and transforming growth factor, thereby aggravating the deposition of extracellular matrix components and promoting the development of hepatic fibrosis (16,35). At present, no studies, to the best of our knowledge, have described whether the integrin complex could participate in the regulation of fibrosis in OXA-induced HSOS. OXA can promote platelet aggregation and adhesion through the release of matrix metalloproteinases and a variety of growth factors, thus leading to the aggravation of hepatic sinusoidal obstruction (16). The arachidonic acid oxidation pathway can be used as a target for the regulation of blood coagulation and platelet activation (42) and also participates in inflammatory reaction (43), which may affect the state of platelet activation in OXA-induced HSOS. Steroid hydroxylase, mainly cytochrome P-450, plays a role in maintaining homeostasis in the synthesis and metabolism of cholesterol and bile acids (44,45). However, no studies related to bile acid and lipid balance in OXA-induced HSOS are available, to the best of our knowledge.

KEGG enrichment analysis of DEGs identified the significantly enriched pathways, which is helpful for identifying biological regulatory pathways with significant differences under experimental conditions. The present study revealed that the DEGs between the control group and the 10 mg/kg OXA group were mostly enriched in pathways related to human diseases. Among the top 30 enriched KEGG pathways, the regulation of 'steroid hormone biosynthesis',
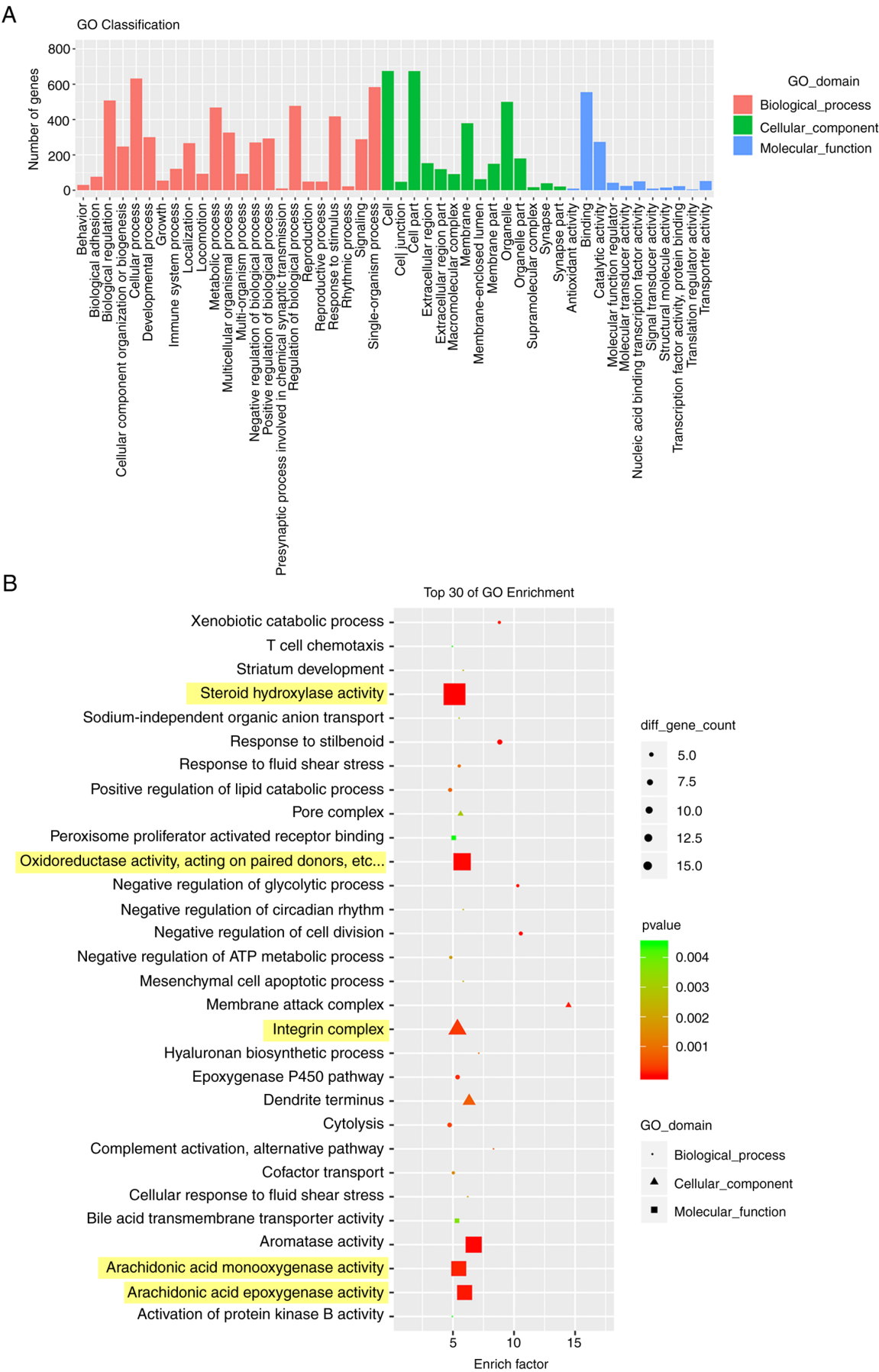
Figure 5. GO function analysis of the livers of mice with OXA-induced hepatic sinusoidal obstruction syndrome. (A) GO enrichment of DEGs in 3 functional groups: Biological Process (red), Cellular Component (green) and Molecular Function(blue).The x-axis represents the significantly enriched GO terms and the y-axis represents the number of DEGs involved in GO terms. (B) Top 30 enriched GO terms. The x-axis represents the enrichment factor of each term and y-axis represents the GO terms. Data are shown for the control and 10 mg/kg OXA groups. GO, Gene Ontology; OXA, oxaliplatin.

A

KEGG Classification

B

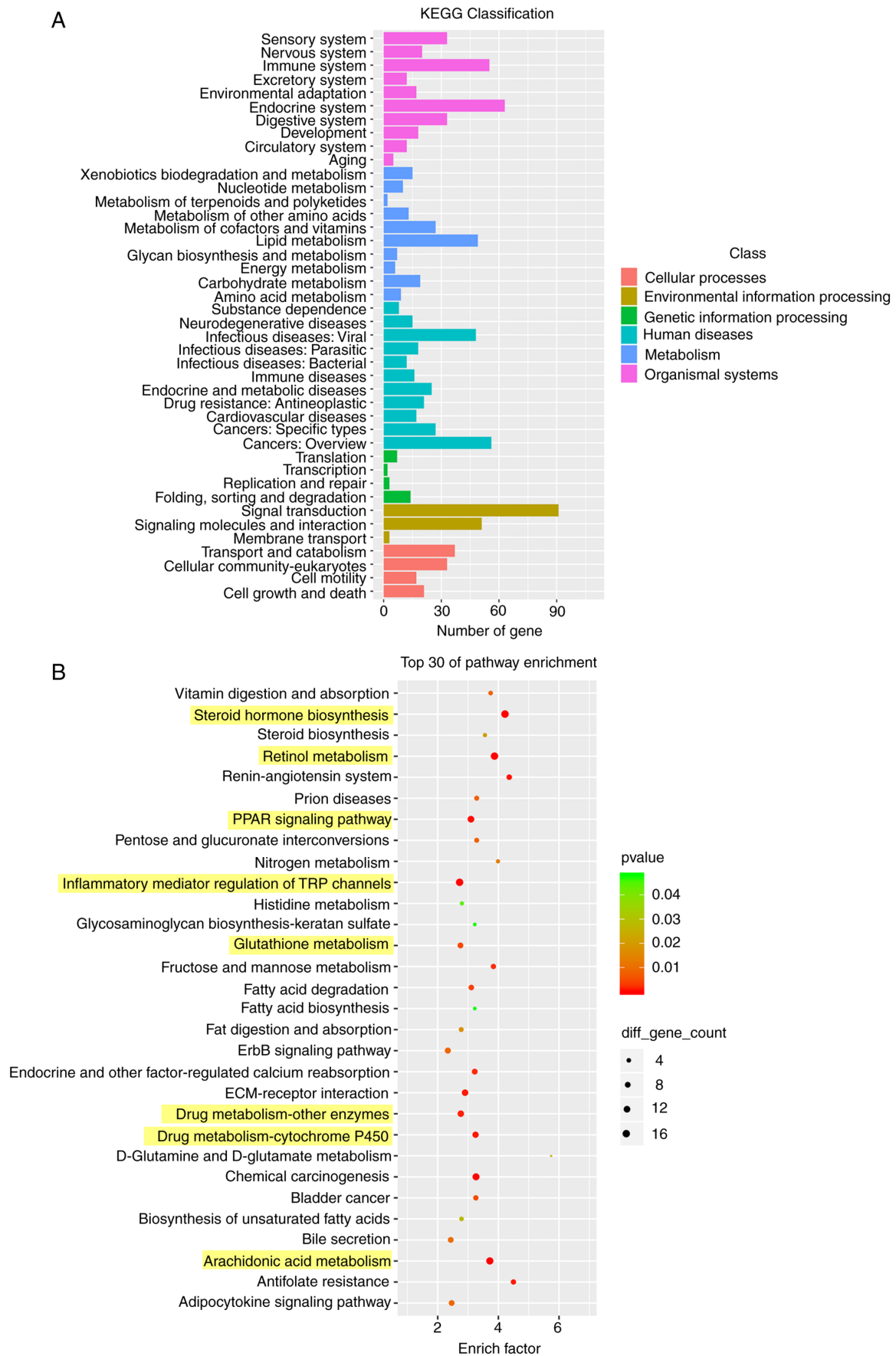### Top 30 of pathway enrichment

Figure 6. KEGG pathway analysis of the livers of mice with OXA-induced hepatic sinusoidal obstruction syndrome. (A) KEGG enrichment of DEGs in 5 pathway groups: Cellular Progress (red), Environmental Information Processing (brown), Genetic Information Processing (green), Human Diseases Metabolism (cyan) and Organismal Systems (pink). The x-axis represents the significantly enriched KEGG pathway groups and the y-axis represents the number of DEGs involved in KEGG pathways. (B) Top 30 KEGG enriched pathways. The x-axis represents the enrichment factor of each pathway and y-axis represents the KEGG pathways. Data are shown for the control and 10 mg/kg OXA groups. KEGG, Kyoto Encyclopedia of Genes and Genomes; OXA, oxaliplatin.
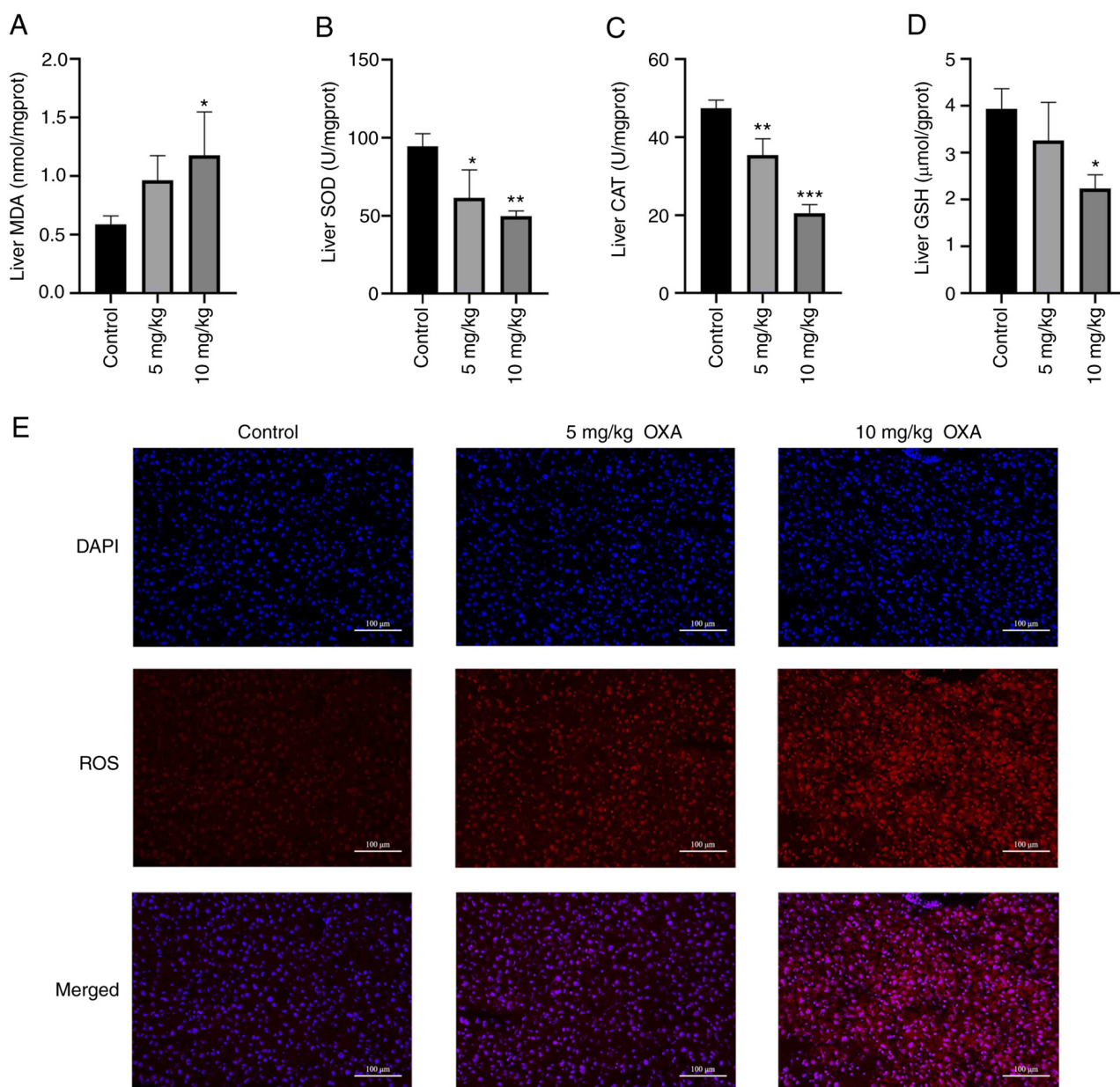
Figure 7. OXA-induced oxidative stress in the liver. (A) MDA levels, and activity of (B) SOD, (C) CAT and (D) GSH in each group of mice were measured. (E) Detection of ROS levels (DHE probe technology; magnification, x400; scale bar=50 μm). Data are shown as the mean ± standard deviation for each group and analyzed with a one-way ANOVA followed by Dunnett's post hoc test. *P<0.05, **P<0.01 and ***P<0.001 vs. control group. OXA, oxaliplatin; MDA, malondialdehyde; CAT, catalase; GSH, reduced glutathione; ROS, reactive oxygen species; DHE, dihydroethidium.

'retinol metabolism', 'drug metabolism cytochrome P450' and 'arachidonic acid metabolism' were consistent with the main functional categories enriched in GO function analysis, which further confirmed their regulatory role in steroid anabolism, changes in coagulation function and ligand activation. Liver inflammation has been considered a possible driving factor for liver damage caused by OXA (16). A previous study demonstrated that in OXA-induced animal models, the inflammatory factors interleukin 16 and C-C motif chemokine ligand 2 were upregulated (46). The microarray results of the present study demonstrated that the inflammatory mediator regulation of TRP channels may serve a role in OXA-induced HSOS, which needs to be further explored.

Notably, 'oxidoreductase activity' in GO analysis and the 'glutathione metabolism' pathway in KEGG analysis indicated

that oxidative stress may be involved in OXA-induced HSOS. The activity of oxidoreductase affects the regulation of redox homeostasis in the body. A previous study (35) preliminarily found that after the injection of OXA, the levels of antioxidant enzymes SOD and glutathione peroxidase were decreased in the liver tissue of mice with nonalcoholic fatty liver disease. Glutathione metabolism affects the changes in ROS levels in a variety of liver diseases and can aggravate the state of oxidative stress (47). Moreover, it has been reported that oxidative stress caused by GSH depletion may be one of the reasons for OXA-induced hepatic sinusoid injury (16). Tabassum *et al* (48) evaluated the GSH content in liver mitochondria after OXA treatment and demonstrated that a decrease in GSH content may be related to the binding of OXA to free or protein-bound sulfhydryl groups. The current study also revealed that after

the long-term administration of OXA, the MDA liver oxidation index in mice increased, whereas the levels of antioxidants SOD, CAT and GSH were significantly decreased. In addition, ROS levels in the liver of mice in the OXA group were increased in a dose-dependent manner, indicating that OXA could lead to an imbalance in the redox system.

Notably, in the present study, GO and KEGG analyses suggested that other pathways may be involved in OXA-induced HSOS, such as mesenchymal cell apoptotic process and bile secretion. Therefore, the data provided novel directions for the study of the pathogenetic mechanisms of OXA-induced HSOS.

There were some limitations to the present study. First, the aim of the present study was to establish an animal model of OXA-induced HSOS, so *in vivo* experiments were preferentially conducted. Corresponding *in vitro* experiments using hepatic sinusoidal endothelial cells to explore the pathogenetic mechanisms of OXA-induced HSOS will be conducted in the future. Second, the symptoms caused by OXA may be associated with its systemic effects, such as pro-inflammatory effects, and effects on the nervous system and circulatory system, which may also aggravate liver injuries and is worth exploring in the future. Third, more advanced detection equipment and indicators, such as ultrasound, angiography and the assessment of portal hypertension, will be employed in the confirmation of HSOS.

In conclusion, the present study established a mouse model of OXA-induced HSOS. Through microarray analysis, it verified the role of the oxidative stress pathway in this disease and identified some potential mechanistic pathways, which could lay the foundation for identifying the mechanisms of OXA-induced HSOS.

Availability of data and materials

The datasets generated and/or analyzed during the current study are available in the Gene Expression Omnibus repository at https://www.ncbi.nlm.nih.gov/geo/query/acc.cgi?acc=GSE211859. All other data sets in the present study are available from the corresponding author on reasonable request.

Authors' contributions

CZhu, DL, XR and CZha designed the study. CZhu, QG and XW performed the experiments. CZhu, XC, DL and PG contributed to the data acquisition and analysis. CZhu wrote the manuscript. CZhu, PG and CZha contributed to the critical revision of the manuscript. CZhu and XC confirm the authenticity of all the raw data. All authors made significant contributions to this study, and all authors read and approved the final manuscript.

Ethics approval and consent to participate

The present study was approved by the Animal Experiment Ethics Committee of Tongji Medical College, Huazhong University of Science and Technology (Wuhan, China; approval no. 2646).

Patient consent for publication

Not applicable.

Competing interests

The authors declare that they have no competing interests.

References

1. Siegel RL, Miller KD and Jemal A: Cancer statistics, 2020. CA Cancer J Clin 70: 7-30, 2020.
2. Soulié P, Raymond E, Brienza S and Cvitkovic E: Oxaliplatin: The first DACH platinum in clinical practice. Bull Cancer 84: 665-673, 1997 (In French).
3. Adam R, Wicherts DA, de Haas RJ, Ciacio O, Lévi F, Paule B, Ducreux M, Azoulay D, Bismuth H and Castaing D: Patients with initially unresectable colorectal liver metastases: Is there a possibility of cure? J Clin Oncol 27: 1829-1835, 2009.
4. Duwe G, Knitter S, Pesthy S, Beierle AS, Bahra M, Schmelzle M, Schmuck RB, Lohneis P, Raschzok N, Öllinger R, et al: Hepatotoxicity following systemic therapy for colorectal liver metastases and the impact of chemotherapy-associated liver injury on outcomes after curative liver resection. Eur J Surg Oncol 43: 1668-1681, 2017.
5. Liang XB, Hou SH, Li YP, Wang LC, Zhang X and Yang J: Irinotecan or oxaliplatin combined with 5-fluorouracil and leucovorin as first-line therapy for advanced colorectal cancer: A meta-analysis. Chin Med J (Engl) 123: 3314-3318, 2010.
6. Puente A, Fortea JI, Del Pozo C, Huelin P, Cagigal ML, Serrano M, Cabezas J, Arias LM, Iruzubieta P, Cuadrado A, et al: Porto-sinusoidal vascular disease associated to oxaliplatin: An entity to think about it. Cells 8: 1506, 2019.
7. André T, Boni C, Navarro M, Tabernero J, Hickish T, Topham C, Bonetti A, Clingan P, Bridgewater J, Rivera F and de Gramont A: Improved overall survival with oxaliplatin, fluorouracil, and leucovorin as adjuvant treatment in stage II or III colon cancer in the MOSAIC trial. J Clin Oncol 27: 3109-3116, 2009.
8. Erdem GU, Dogan M, Demirci NS and Zengin N: Oxaliplatin-induced acute thrombocytopenia. J Cancer Res Ther 12: 509-514, 2016.
9. Zhao J, van Mierlo K, Gomez-Ramirez J, Kim H, Pilgrim CHC, Pessaux P, Rensen SS, van der Stok EP, Schaap FG, Soubrane O, et al: Systematic review of the influence of chemotherapy-associated liver injury on outcome after partial hepatectomy for colorectal liver metastases. Br J Surg 104: 990-1002, 2017.
10. Rubbia-Brandt L, Audard V, Sartoretti P, Roth AD, Brezault C, Le Charpentier M, Dousset B, Morel P, Soubrane O, Chaussade S, et al: Severe hepatic sinusoidal obstruction associated with oxaliplatin-based chemotherapy in patients with metastatic colorectal cancer. Ann Oncol 15: 460-466, 2004.
11. Nassereddine S, Alsubait S and Tabbara I: Sinusoidal obstruction syndrome (veno-occlusive disease) following hematopoietic stem cell transplant: Insights and therapeutic advances. Anticancer Res 38: 2597-2605, 2018.
12. Nam SJ, Cho JY, Lee HS, Choe G, Jang JJ, Yoon YS, Han HS and Kim H: Chemotherapy-associated hepatopathy in korean colorectal cancer liver metastasis patients: Oxaliplatin-based chemotherapy and sinusoidal injury. Korean J Pathol 46: 22-29, 2012.

13. Rubbia-Brandt L, Lauwers GY, Wang H, Majno PE, Tanabe K, Zhu AX, Brezault C, Soubrane O, Abdalla EK, Vauthey JN, *et al*: Sinusoidal obstruction syndrome and nodular regenerative hyperplasia are frequent oxaliplatin-associated liver lesions and partially prevented by bevacizumab in patients with hepatic colorectal metastasis. Histopathology 56: 430-439, 2010.
14. Fan CQ and Crawford JM: Sinusoidal obstruction syndrome (hepatic veno-occlusive disease). J Clin Exp Hepatol 4: 332-346, 2014.
15. Russolillo N, Langella S, Perotti S, Lo Tesoriere R, Forchino F and Ferrero A: Preoperative assessment of chemotherapeutic associated liver injury based on indocyanine green retention test. Int J Surg 31: 80-85, 2016.
16. Zhu C, Ren X, Liu D and Zhang C: Oxaliplatin-induced hepatic sinusoidal obstruction syndrome. Toxicology 460: 152882, 2021.
17. Overman MJ, Maru DM, Charnsangavej C, Loyer EM, Wang H, Pathak P, Eng C, Hoff PM, Vauthey JN, Wolff RA and Kopetz S: Oxaliplatin-mediated increase in spleen size as a biomarker for the development of hepatic sinusoidal injury. J Clin Oncol 28: 2549-2555, 2010.
18. Cayet S, Pasco J, Dujardin F, Besson M, Orain I, De Muret A, Miquelestorena-Standley E, Thiery J, Genet T and Le Bayon AG: Diagnostic performance of contrast-enhanced CT-scan in sinusoidal obstruction syndrome induced by chemotherapy of colorectal liver metastases: Radio-pathological correlation. Eur J Radiol 94: 180-190, 2017.
19. Han NY, Park BJ, Kim MJ, Sung DJ and Cho SB: Hepatic parenchymal heterogeneity on contrast-enhanced CT scans following oxaliplatin-based chemotherapy: Natural history and association with clinical evidence of sinusoidal obstruction syndrome. Radiology 276: 766-774, 2015.
20. Couto M and Cates C: Laboratory guidelines for animal care. Methods Mol Biol 1920: 407-430, 2019.
21. Livak KJ and Schmittgen TD: Analysis of relative gene expression data using real-time quantitative PCR and the 2(-Delta Delta C(T)) method. Methods 25: 402-408, 2001.
22. Lu Y, Wu S, Xiang B, Li L and Lin Y: Curcumin attenuates oxaliplatin-induced liver injury and oxidative stress by activating the Nrf2 pathway. Drug Des Devel Ther 14: 73-85, 2020.
23. Li X, Zhang ZS, Zhang XH, Yang SN, Liu D, Diao CR, Wang H and Zheng FP: Cyanidin inhibits EMT induced by oxaliplatin via targeting the PDK1-PI3K/Akt signaling pathway. Food Funct 10: 592-601, 2019.
24. Miyagi A, Kawashiri T, Shimizu S, Shigematsu N, Kobayashi D and Shimazoe T: Dimethyl fumarate attenuates oxaliplatin-induced peripheral neuropathy without affecting the anti-tumor activity of oxaliplatin in rodents. Biol Pharm Bull 42: 638-644, 2019.
25. Rubbia-Brandt L, Tauzin S, Brezault C, Delucinge-Vivier C, Descombes P, Dousset B, Majno PE, Mentha G and Terris B: Gene expression profiling provides insights into pathways of oxaliplatin-related sinusoidal obstruction syndrome in humans. Mol Cancer Ther 10: 687-696, 2011.
26. Zou X, Wang Y, Peng C, Wang B, Niu Z, Li Z and Niu J: Magnesium isoglycyrrhizinate has hepatoprotective effects in an oxaliplatin-induced model of liver injury. Int J Mol Med 42: 2020-2030, 2018.
27. Kim MJ, Han SW, Lee DW, Cha Y, Lee KH, Kim TY, Oh DY, Kim SH, Im SA, Bang YJ and Kim TY: Splenomegaly and its associations with genetic polymorphisms and treatment outcome in colorectal cancer patients treated with adjuvant FOLFOX. Cancer Res Treat 48: 990-997, 2016.
28. El Chediak A, Haydar AA, Hakim A, Massih SA, Hilal L, Mukherji D, Temraz S and Shamseddine A: Increase in spleen volume as a predictor of oxaliplatin toxicity. Ther Clin Risk Manag 14: 653-657, 2018.
29. Zhang YF, Huang Y, Ni YH and Xu ZM: Systematic elucidation of the mechanism of geraniol via network pharmacology. Drug Des Devel Ther 13: 1069-1075, 2019.
30. Tsikas D: Assessment of lipid peroxidation by measuring malondialdehyde (MDA) and relatives in biological samples: Analytical and biological challenges. Anal Biochem 524: 13-30, 2017.
31. Nordlinger B, Sorbye H, Glimelius B, Poston GJ, Schlag PM, Rougier P, Bechstein WO, Primrose JN, Walpole ET, Finch-Jones M, *et al*: Perioperative FOLFOX4 chemotherapy and surgery versus surgery alone for resectable liver metastases from colorectal cancer (EORTC 40983): Long-term results of a randomised, controlled, phase 3 trial. Lancet Oncol 14: 1208-1215, 2013.
32. Vreuls CP, Van Den Broek MA, Winstanley A, Koek GH, Wisse E, Dejong CH, Olde Damink SW, Bosman FT and Driessen A: Hepatic sinusoidal obstruction syndrome (SOS) reduces the effect of oxaliplatin in colorectal liver metastases. Histopathology 61: 314-318, 2012.
33. Tajima H, Ohta T, Miyashita T, Nakanuma S, Matoba M, Miyata T, Sakai S, Okamoto K, Makino I, Kinoshita J, *et al*: Oxaliplatin-based chemotherapy induces extravasated platelet aggregation in the liver. Mol Clin Oncol 3: 555-558, 2015.
34. Robinson SM, Mann J, Vasilaki A, Mathers J, Burt AD, Oakley F, White SA and Mann DA: Pathogenesis of FOLFOX induced sinusoidal obstruction syndrome in a murine chemotherapy model. J Hepatol 59: 318-326, 2013.
35. Lu Y, Lin Y, Huang X, Wu S, Wei J and Yang C: Oxaliplatin aggravates hepatic oxidative stress, inflammation and fibrosis in a non-alcoholic fatty liver disease mouse model. Int J Mol Med 43: 2398-2408, 2019.
36. Yang L, Ding Y, Rao S, Chen C and Zeng M: T_1 mapping on Gd-EOB-DTPA-enhanced MRI for the prediction of oxaliplatin-induced liver injury in a mouse model. J Magn Reson Imaging 53: 896-902, 2021.
37. Oneda E and Zaniboni A: Adjuvant treatment of colon cancer with microsatellite instability-the state of the art. Crit Rev Oncol Hematol 169: 103537, 2022.
38. Xia T, Zhang J, Han L, Jin Z, Wang J, Li X, Man S, Liu C and Gao W: Protective effect of magnolol on oxaliplatin-induced intestinal injury in mice. Phytother Res 33: 1161-1172, 2019.
39. Valla DC and Cazals-Hatem D: Sinusoidal obstruction syndrome. Clin Res Hepatol Gastroenterol 40: 378-385, 2016.
40. McCarty JH: $\alpha v \beta 8$ integrin adhesion and signaling pathways in development, physiology and disease. J Cell Sci 133: jcs239434, 2020.
41. Munger JS, Huang X, Kawakatsu H, Griffiths MJ, Dalton SL, Wu J, Pittet JF, Kaminski N, Garat C, Matthay MA, *et al*: The integrin alpha v beta 6 binds and activates latent TGF beta 1: A mechanism for regulating pulmonary inflammation and fibrosis. Cell 96: 319-328, 1999.
42. Trostchansky A, Moore-Carrasco R and Fuentes E: Oxidative pathways of arachidonic acid as targets for regulation of platelet activation. Prostaglandins Other Lipid Mediat 145: 106382, 2019.
43. Capdevila JH, Falck JR and Harris RC: Cytochrome P450 and arachidonic acid bioactivation. Molecular and functional properties of the arachidonate monooxygenase. J Lipid Res 41: 163-181, 2000.
44. Sheets JJ, Mason JI, Wise CA and Estabrook RW: Inhibition of rat liver microsomal cytochrome P-450 steroid hydroxylase reactions by imidazole antimycotic agents. Biochem Pharmacol 35: 487-491, 1986.
45. Pikuleva IA: Cholesterol-metabolizing cytochromes P450. Drug Metab Dispos 34: 513-520, 2006.
46. Jarzabek MA, Proctor WR, Vogt J, Desai R, Dicker P, Cain G, Raja R, Brodbeck J, Stevens D, van der Stok EP, *et al*: Interrogation of transcriptomic changes associated with drug-induced hepatic sinusoidal dilatation in colorectal cancer. PLoS One 13: e198099, 2018.
47. Lu SC, Mato JM, Espinosa-Diez C and Lamas S: MicroRNA-mediated regulation of glutathione and methionine metabolism and its relevance for liver disease. Free Radic Biol Med 100: 66-72, 2016.
48. Tabassum H, Waseem M, Parvez S and Qureshi MI: Oxaliplatin-induced oxidative stress provokes toxicity in isolated rat liver mitochondria. Arch Med Res 46: 597-603, 2015.